

Observation of $Y(2175)$ in $J/\psi \rightarrow \eta\phi f_0(980)$

X. Wan X.Y. Shen F. Liu

September 13, 2007

Abstract

The decays of $J/\psi \rightarrow \eta\phi f_0(980)$ ($\eta \rightarrow \gamma\gamma, \phi \rightarrow K^+K^-, f_0(980) \rightarrow \pi^+\pi^-$) are analyzed using a sample of 5.8×10^7 J/ψ events collected with BESII detector at Beijing Electron-Positron Collider (BEPC). A structure at around $2.19 \text{ GeV}/c^2$ with about 5σ significance is observed in the $\phi f_0(980)$ invariant mass spectrum. A fit with a Breit-Wigner function gives the peak mass and width of $m = 2.186 \pm 0.010(\text{stat}) \pm 0.005(\text{syst}) \text{ GeV}/c^2$ and $\Gamma = 0.065 \pm 0.023(\text{stat}) \pm 0.006(\text{syst}) \text{ GeV}/c^2$, respectively, that are consistent with those of $Y(2175)$, observed by BABAR collaboration in the initial-state radiation(ISR) process $e^+e^- \rightarrow \gamma_{ISR}\phi f_0(980)$. The production branching ratio is determined to be $Br(J/\psi \rightarrow \eta Y(2175)) \cdot Br(Y(2175) \rightarrow \phi f_0(980)) \cdot Br(f_0(980) \rightarrow \pi^+\pi^-) = (3.06 \pm 0.71(\text{stat}) \pm 0.45(\text{syst})) \times 10^{-4}$, if assuming $Y(2175)$ a 1^{--} state.

1 Introduction

Recently the BABAR collaboration observed a new 1^{--} structure with mass $m = 2.175 \pm 0.010 \pm 0.015 \text{ GeV}/c^2$ and width $\Gamma = 58 \pm 16 \pm 20 \text{ MeV}/c^2$, respectively [1]. This structure is denoted as $Y(2175)$ and is interpreted as a hybrid[2], a $2^3D_1 s\bar{s}$ state[3], or a $s\bar{s}s\bar{s}$ tetraquark[4], *etc.*. In this analysis, we report the observation of $Y(2175)$ in the decays of $J/\psi \rightarrow \eta\phi f_0(980)$, with $\eta \rightarrow \gamma\gamma, \phi \rightarrow K^+K^-, f_0(980) \rightarrow \pi^+\pi^-$, using a sample of 5.8×10^7 J/ψ events collected with BESII detector at Beijing Electron-Positron Collider (BEPC).

2 BES Detector

The Beijing Spectrometer(BES)[5] is a conventional cylindrical magnetic detector at Beijing Electron-Positron Collider(BEPC)[6]. A 12-layer Vertex Chamber (VC) surrounds the beryllium beam pipe and provides trigger information, as well as coordinate information. A forty-layer main drift chamber (MDC) located just outside the VC yields precise measurements of charged particle trajectories with a solid angle coverage over 85% of 4π ; it also provides ionization energy loss (dE/dx) measurements which are used for particle identification. Momentum resolution of $1.7\%\sqrt{1+p^2}$ (p in GeV/ c) and dE/dx resolution for hadron tracks of $\sim 8\%$ are obtained. An array of 48 scintillation counters surrounding the MDC measures the time of flight (TOF) of charged particles with a resolution of about 200 ps for hadrons. Outside the TOF counters, a 12 radiation length, lead-gas barrel shower counter (BSC), operating in self quenching streamer mode, measures the energies of electrons and photons over 80% of the total solid angle with an energy resolution of $\sigma_E/E = 0.22/\sqrt{E}$ (E in GeV). Outside the solenoidal coil, which provides a 0.4 t magnetic field over the tracking volume, is an iron flux return that is instrumented with three double-layer muon counters that identify muons with momentum greater than 500 MeV/ c .

In this analysis, a GEANT3 based Monte Carlo package (SIMBES[7]) with detailed consideration of the detector performance is used. The consistency between data and Monte Carlo has been carefully checked in many high purity physics channels, and the agreement is reasonable, as described in detail in Ref.[7]. For $J/\psi \rightarrow \eta Y(2175)$ ($Y(2175) \rightarrow \phi f_0(980)$, $f_0(980) \rightarrow \pi\pi$), supposing J^{PC} of $Y(2175)$ is 1^{--} , the Monte-Carlo generator which considers the angular distributions of $1^{--} \rightarrow 0^{-+} + 1^{--}$, $1^{--} \rightarrow 1^{--} + 0^{++}$ is used to estimate the detection efficiency.

3 Event Selection

About 58 million J/ψ data which were collected from the November of 1999 to the April of 2001 are used in this analysis. At first, the J/ψ runs with poor data quality are filtered out.

3.1 Initial event selection

3.1.1 Charged Track Selection

The good charged tracks should satisfy the following criteria:

- The charged track is reconstructed from MDC
- Good Helix fit for each track $M_{fit} = 2$
- Electric charge of each track $Q = +1$ or -1
- Originate from the interaction point $\sqrt{x_0^2 + y_0^2} < 0.02m$, $|z_0| < 0.2m$

The number of good charged tracks which satisfy above criteria is required to be four and the net charge of four charged tracks is zero. The good charged tracks should also satisfy the following cuts :

- Transverse momentum $P_{xy} > 70\text{MeV}/c$
- The cosine of polar angle of each track $|\cos\theta| < 0.8$

3.1.2 Photon Selection

- Hit BSC ; first hit layer > 6 and total hit layers number > 1 ,
- Energy deposited in the BSC $E_\gamma > 60\text{MeV}$.
- The angle between the direction at the first layer of BSC and the developing direction of clustering is greater than 30° .
- The angle between photon and its nearest charged tracks is greater than 5° .
- If the invariant mass of two photons is less than $50\text{MeV}/c^2$ and the angle between two photons is less than 10° , the photon with smaller energy is regarded as splitting from the other photon and is rejected. Its energy is added to the bigger one.

3.1.3 Particle Identification

In this analysis, the charged particles in final state are pions or kaons. To identify them from other charged particles, we define:

$$\chi_{TOF}(i) = \frac{TOF_{measure} - TOF_{expected-i}}{\sigma_{TOF-i}}$$

$$\chi_{dE/dx}(i) = \frac{dE/dx_{measure} - dE/dx_{expected-i}}{\sigma_{dE/dx-i}} \quad (P_{track} < 0.8 \text{ GeV}/c)$$

where i denotes the desired hypothesis which is π , K or p . The TOF and dE/dx information are combined to identify particles.

$$\chi^2(i) = \chi_{TOF}^2(i) + \chi_{dE/dx}^2(i) \quad (1)$$

- To identify a pion, it is required that $\chi^2(\pi) < \chi^2(K)$ and $\chi^2(\pi) < \chi^2(p)$.
- To identify a kaon, it is required that $\chi^2(K) < \chi^2(\pi)$ and $\chi^2(K) < \chi^2(p)$.

3.2 Final event selection

Events with four good charged tracks and at least two good photons are selected. The four charged tracks are required to consist of an unambiguously identified $K^+K^-\pi^+\pi^-$ combination. All photons are paired for 4C fit in the $K^+K^-\pi^+\pi^-\gamma\gamma$ hypothesis and the two photons with the smallest $\chi^2_{K^+K^-\pi^+\pi^-\gamma\gamma}$ value are tagged. The events with the smallest $\chi^2_{K^+K^-\pi^+\pi^-\gamma\gamma}$ are retained and $\chi^2_{K^+K^-\pi^+\pi^-\gamma\gamma} < 15$ is required. Fig. 1 shows the distribution, in which the crosses are for the data and the histogram is for the sum of Monte Carlo signal events and background events estimated from sidebands.

In $\gamma\gamma$ invariant mass spectrum, π^0 and η are observed (shown in Fig. 2). When K^+K^- and $\pi^+\pi^-$ invariant masses are required to be in ϕ and $f_0(980)$ regions, the η signal becomes much clearer than π_0 , and the backgrounds are greatly reduced. Candidate η mesons are selected by requiring $|m_{\gamma\gamma} - 0.547| < 0.037\text{GeV}/c^2$ (shown in Fig. 3).

In K^+K^- invariant mass spectrum, the ϕ signal is distinct (shown in Fig. 4). After the mass cut of η and $f_0(980)$, the backgrounds become little. Candidate ϕ mesons are selected by requiring $|m_{K^+K^-} - 1.02| < 0.019\text{GeV}/c^2$ (shown in Fig. 5).

The $f_0(980)$ signal is not clear in $\pi^+\pi^-$ invariant mass spectrum until η and ϕ invariant mass cuts are applied (shown in Fig. 6). Candidate $f_0(980)$ mesons are required by $|m_{\pi^+\pi^-} - 0.980| < 0.06\text{GeV}/c^2$ (shown in Fig. 7).

It is worthy to mention that the above major selection criteria are optimized jointly by maximizing $\frac{S}{\sqrt{S+B}}$, where S is the expected signal events which is proportional to signal efficiency (to avoid the bias in the invariant mass spectrum, the signal sample is generated with the MC simulation process $J/\psi \rightarrow \eta\phi f_0(980)$ (not $J/\psi \rightarrow \eta Y(2175), Y(2175) \rightarrow \phi f_0(980)$) in the optimization procedure), and S+B represents the total number of selected events from data.

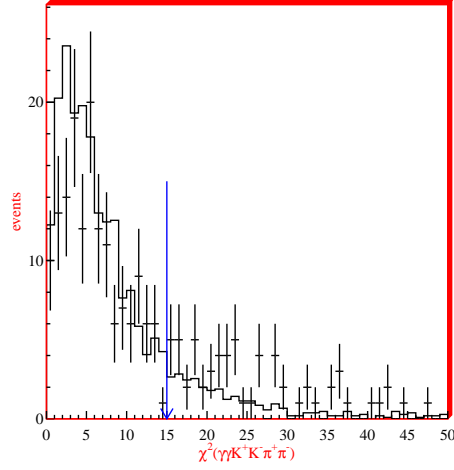


Figure 1: The distribution of $\chi^2(\gamma\gamma K^+ K^- \pi^+ \pi^-)$. The crosses are for data and the histogram is for the sum of Monte Carlo signal events and background events estimated from sidebands.

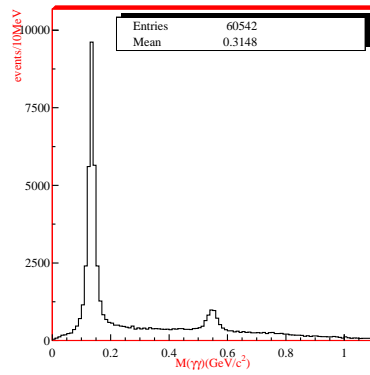


Figure 2: The $\gamma\gamma$ invariant mass spectrum

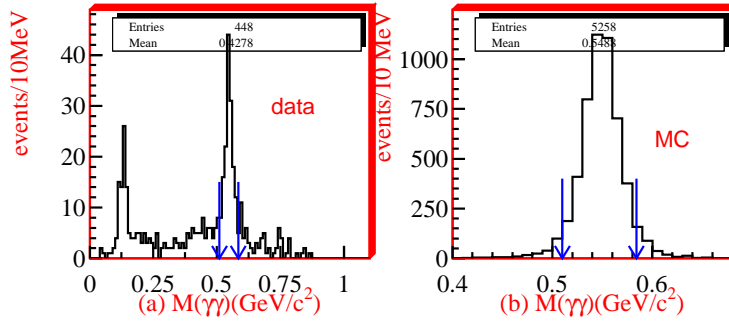


Figure 3: The $\gamma\gamma$ invariant mass spectrum after the mass cuts of ϕ and $f_0(980)$. (a) is for data and (b) for MC. Arrows on the plot represent cut criteria.

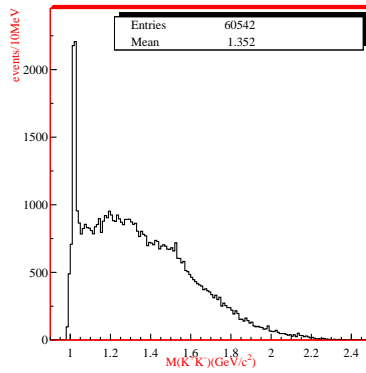


Figure 4: The K^+K^- invariant mass spectrum

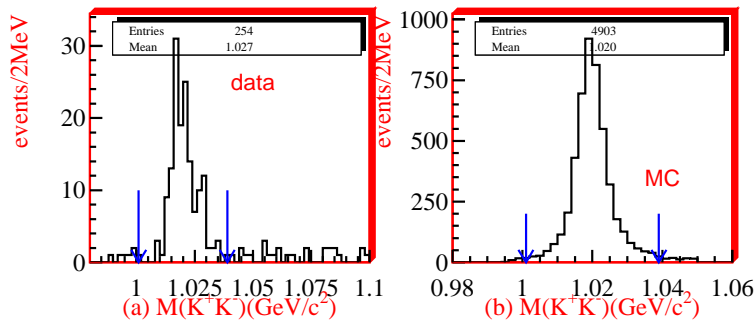


Figure 5: The K^+K^- invariant mass spectrum after the mass cuts of η and $f_0(980)$. (a) is for data and (b) for MC. Arrows on the plot represent cut criteria.

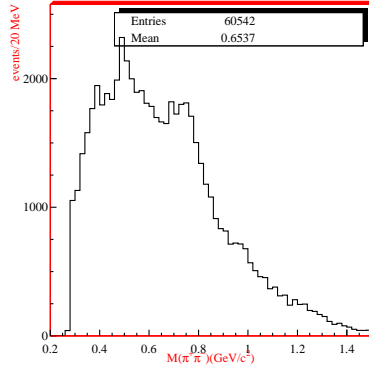


Figure 6: The $\pi^+\pi^-$ invariant mass spectrum

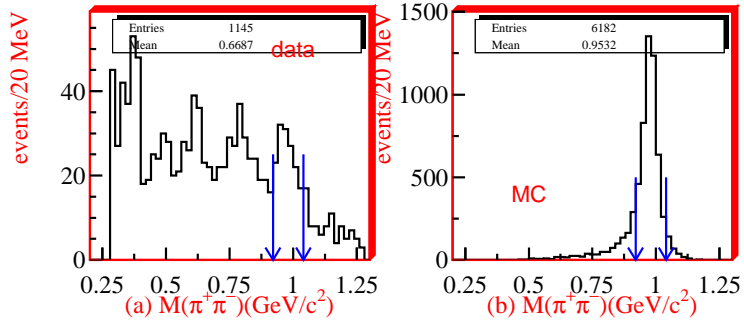


Figure 7: The $\pi^+\pi^-$ invariant mass spectrum after the mass cuts of η and ϕ . (a) is for data and (b) for MC. Arrows on the plot represent cut criteria.

4 $\phi f_0(980)$ invariant mass spectrum

After above criteria, a total of 152 events are retained. The $\phi f_0(980)$ invariant mass spectrum for these events is shown in Fig. 8, where a structure at around 2.19 GeV/c² is observed. No structure around 2.19 GeV/c² is seen in a sample of $J/\psi \rightarrow \eta \phi f_0(980)$ MC events generated with a uniform phase-space generator (shown in Fig. 9). Fig. 10 is the plot of efficiency versus $\phi f_0(980)$ invariant mass and the curve is a 4th-order polynomial fit. Mass dependence around 2.19 GeV/c² region is small. This efficiency curve is included in later fit.

The Dalitz plots of $m_{\eta f_0(980)}^2$ versus $m_{\eta \phi}^2$ from data and MC sample are shown in Fig. 11 and Fig. 12, respectively. The MC sample obtained here is the sum of the events from $J/\psi \rightarrow \eta Y(2175)(Y(2175) \rightarrow \phi f_0(980), f_0(980) \rightarrow \pi\pi)$ process, generated by assuming J^{PC} of $Y(2175)$ being 1^{--} and considering the angular distributions, and the events from $J\psi \rightarrow \eta \phi f_0(980)$ phase space process.

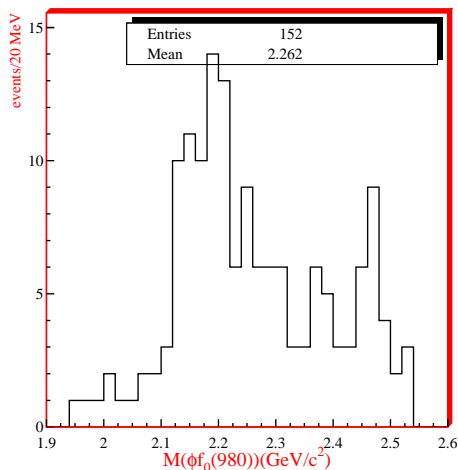


Figure 8: The $\phi f_0(980)$ invariant mass spectrum

5 Background analysis

To clarify where the structure is from, we perform a background analysis through following three ways: (1) study the backgrounds from sidebands. The Backgrounds not from ϕ are estimated from ϕ sidebands. The back-

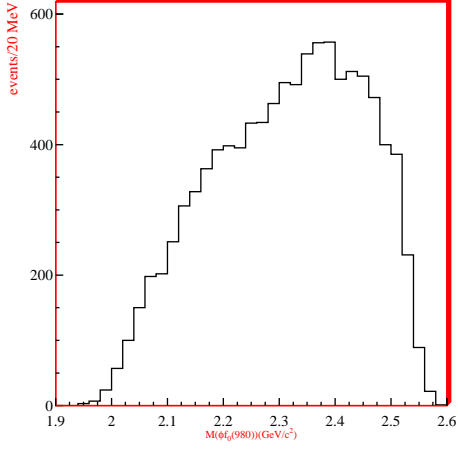


Figure 9: The $\phi f_0(980)$ invariant mass spectrum for phase space events of Monte Carlo simulation.

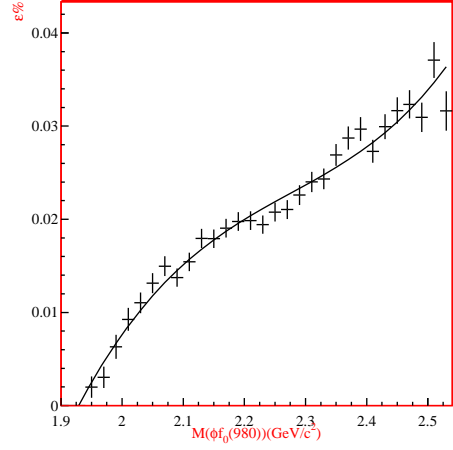


Figure 10: The efficiency vs. $\phi f_0(980)$ mass for $J/\psi \rightarrow \eta \phi f_0(980)$. The curve is the fit.

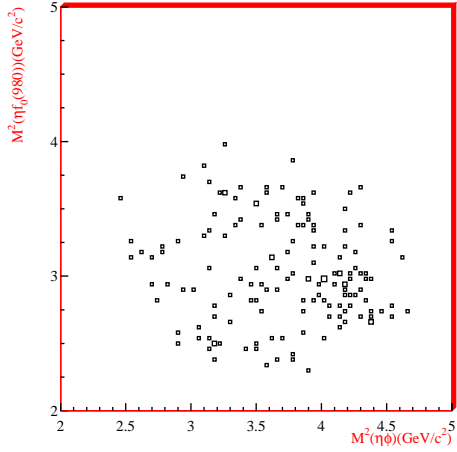


Figure 11: The $m_{\eta f_0(980)}^2$ versus $m_{\eta\phi}^2$ Dalitz plot for data.

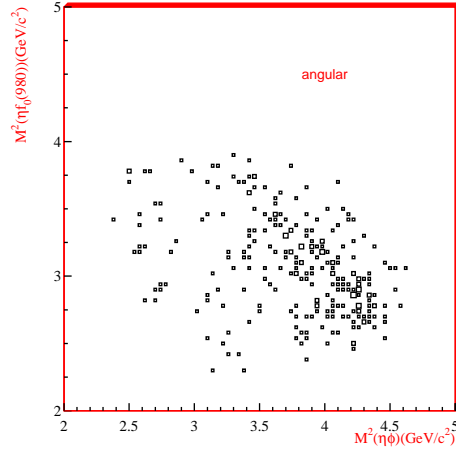


Figure 12: The $m_{\eta f_0(980)}^2$ versus $m_{\eta\phi}^2$ dalitz plot for MC sample. The generated MC sample is described in the text.

ground not from η or $f_0(980)$ are estimated from 2-dimensional $\pi^+\pi^-$ versus $\gamma\gamma$ scatter plot. (2) $J/\psi \rightarrow$ anything MC events. (3) Possible background channels listed in Particle Data Group Tables [13].

5.1 Sidebands

The sidebands of ϕ is obtained by requiring $-0.038\text{GeV}/c^2 < (m_{K^+K^-} - 1.02) < -0.019\text{ GeV}/c^2$ and $0.038\text{GeV}/c^2 < (m_{K^+K^-} - 1.02) < -0.057\text{GeV}/c^2$ (shown in Fig. 13). The invariant mass spectrum of $K^+K^-f_0(980)$ with the invariant mass of K^+K^- being in ϕ sideband region is shown as the histogram in Fig. 14. No evidence of $Y(2175)$ is observed.

The $m_{\pi^+\pi^-}$ versus $m_{\gamma\gamma}$ scatter plot is shown in Fig. 15(a). In the scatter plot, there are four different regions labeled as '1', '2', '3' and '4'.

- $\eta f_0(980)$ region : $|m_{\gamma\gamma} - 0.547| < 0.037\text{ GeV}/c^2$ and $|m_{\pi^+\pi^-} - 0.980| < 0.06\text{GeV}/c^2$
- η sideband region: $0.074\text{GeV}/c^2 < |m_{\gamma\gamma} - 0.547| < 0.111\text{GeV}/c^2$ and $|m_{\pi^+\pi^-} - 0.980| < 0.06\text{GeV}/c^2$
- $f_0(980)$ sideband region: $0.09\text{GeV}/c^2 < |m_{\pi^+\pi^-} - 0.980| < 0.15\text{GeV}/c^2$ and $|m_{\gamma\gamma} - 0.547| < 0.037\text{GeV}/c^2$
- corner region: $0.074\text{GeV}/c^2 < |m_{\gamma\gamma} - 0.547| < 0.111\text{GeV}/c^2$ and $0.09\text{GeV}/c^2 < |m_{\pi^+\pi^-} - 0.980| < 0.15\text{ GeV}/c^2$.

The $\pi^+\pi^-K^+K^-$ spectrum from events in '2', '3' and '4' regions are shown in Fig. 15(b),(c),(d). If linear relationship of $\gamma\gamma$ and $\pi^+\pi^-$ invariant mass distribution around $\eta - f_0(980)$ is assumed, the background contribution from η and $f_0(980)$ sidebands are estimated by '2'+ '3' - '4'. In Fig. 16, the solid histogram shows the $K^+K^-\pi^+\pi^-$ invariant mass distribution in $\eta f_0(980)$ signal region. The hatched histogram shows the background contribution estimated by '2'+ '3'-'4', and no structure around $2.19\text{ GeV}/c^2$ is evident here.

If the linear relationship of invariant mass distribution around η , $f_0(980)$ and ϕ regions is assumed, the total background contribution can be calculated in the following steps:

- 1, adding their single sidebands together.
- 2, subtracting $\eta - f_0(980)$, $\eta - \phi$, $f_0(980) - \phi$ corner region events.
- 3, adding $\eta - f_0(980) - \phi$ three sidebands intersection region events.

The hatched histogram in Fig. 17 shows the total background contribution evaluated by this method. No structure around $2.19 \text{ GeV}/c^2$ is evident.

5.2 $J/\psi \rightarrow$ anything Monte-carlo sample

The $\phi f_0(980)$ invariant mass spectrum from $J/\psi \rightarrow$ anything events generated by LUND-CHARM generator[8] is shown in Fig. 18. The same criteria used in data is applied to this sample. There is no evidence of the structure at $2.19 \text{ GeV}/c^2$.

5.3 Exclusive background channels

The backgrounds are also carefully checked by possible exclusive channels which are listed in PDG06 table. The backgrounds can be separated into 3 classes: (1) include $\phi \rightarrow K^+K^-$, shown in Table. 1; (2) include $\eta \rightarrow \pi^+\pi^-$, shown in Table. 2; (3) not include $\phi \rightarrow K^+K^-$ and $\eta \rightarrow \pi^+\pi^-$, shown in Table. 3.

From the above tables, the background events that survive the selection criteria can be ignored.

6 Results from invariant mass spectrum fitting

The $\phi f_0(980)$ invariant mass spectrum is fitted using one resonance and two resonances, respectively.

6.1 Fitting with one resonance

When fitting with one resonance, different background functions are tried.

6.1.1 Using sidebands contribution as background shape

In this section, we fit the $\phi f_0(980)$ invariant mass spectrum and the total sidebands simultaneously to restrict their background functions being the same. The procedure is like this, firstly we fit the sidebands histogram to get a 3-order polynomial (shown in Fig.19). Secondly we use the polynomial as background function both for the $\phi f_0(980)$ invariant mass spectrum

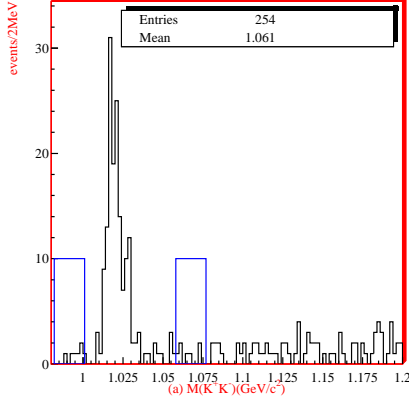


Figure 13: the K^+K^- invariant mass distribution, the boxes represent sidebands region.

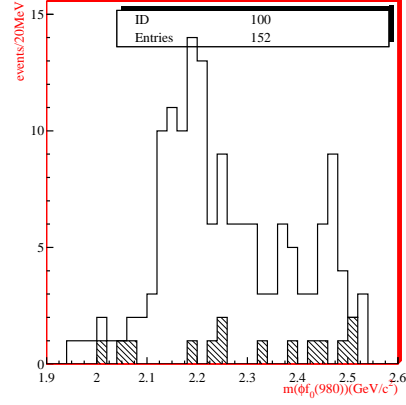


Figure 14: the $\phi f_0(980)$ invariant mass distribution from background events evaluated by ϕ sidebands (hatched histogram) .

Table 1: Exclusive background channels with $\phi \rightarrow K^+K^-$

Decay mode	Br (10^{-4})	MC (10^4)	Residual /efficiency(%)	Norm number
$\gamma\phi\phi \rightarrow \gamma(K^+K^-)(\rho\pi \text{ or } 3\pi)$	0.301	5	0/0	0
$\gamma\phi\omega \rightarrow \gamma(K^+K^-)(\pi^+\pi^-\pi^0)$	1.07	30	0/0	0
$\phi f_2(1525) \rightarrow (K^+K^-)(K_s K_s)$, $K_s \rightarrow \pi^0\pi^0, K_s \rightarrow \pi^+\pi^-$	0.185	5	0/0	0
$\phi K_s K_s$ (exclude $\phi f_2(1525)$)	1.125	5	0/0	0
$\phi\eta'(958) \rightarrow (K^+K^-)(\pi^0\pi^0\eta)$	0.41	5	0/0	0
$\phi\eta'(958) \rightarrow (K^+K^-)(\pi^0\pi^0\eta)$, $\eta \rightarrow \pi^0\pi^0\pi^0$	0.285	1.5	0/0	0
$\phi K_s K^\pm K^\mp, K_s \rightarrow \pi^0\pi^0$	1.083	1	0/0	0
$\phi K^+K^-\pi^0 + \text{c.c.} \rightarrow (K^+K^-K^+K^-\pi^0) + \text{c.c.}$	3.5	10	0/0	0
$\phi K^{*+}K^- + \text{c.c.} \rightarrow (K^+K^-K^+\pi^0K^-) + \text{c.c.}$	1.67	2	0/0	0
$\phi f_1(1285) \rightarrow (K^+K^-)(\pi^+\pi^-\pi^0\pi^0)$	0.28	10	0/0	0

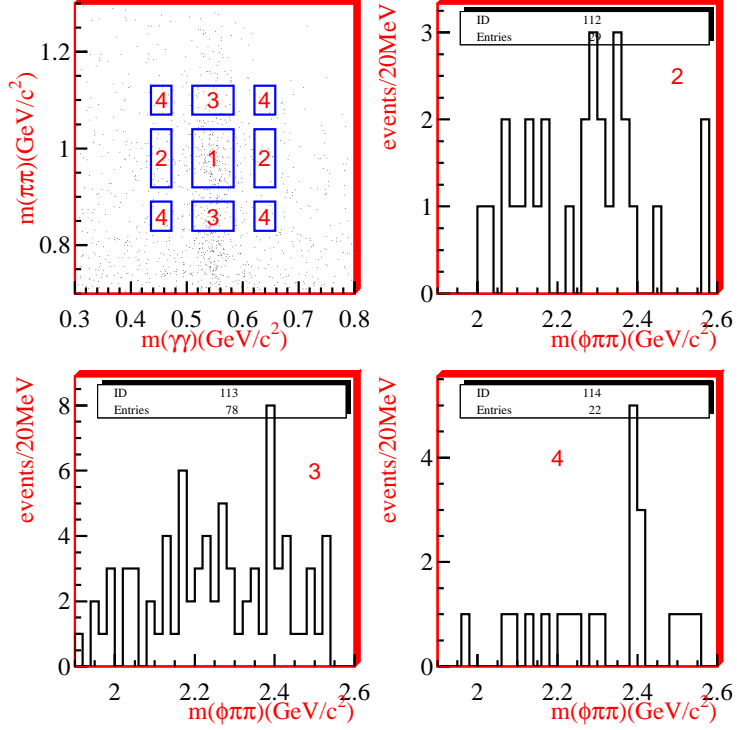


Figure 15: (a) Scatter plot of $m_{\pi^+\pi^-}$ vs. $m_{\gamma\gamma}$ for all selected $\pi^+\pi^-\gamma\gamma$ events. '1' is for $\eta f_0(980)$ signal region; '2' is for η sidebands region; '3' is for $f_0(980)$ sidebands region; '4' is for corner region. (b) The $K^+K^-\pi^+\pi^-$ invariant mass distribution for events in η sidebands region. (c) The $K^+K^-\pi^+\pi^-$ invariant mass distribution for events in $f_0(980)$ sidebands region. (d) The $K^+K^-\pi^+\pi^-$ invariant mass distribution for events in corner region.

Table 2: Background channels with $\eta \rightarrow \gamma\gamma$

Decay mode	Br (10^{-4})	MC (10^4)	Residual /efficiency(%)	Norm number
$\gamma\eta_c \rightarrow \gamma\eta\pi^+\pi^-\eta' \rightarrow \eta\pi^+\pi^-$	0.62	5	0/0	0
$\phi\eta' \rightarrow (\pi^+\pi^-\pi^0)(\pi^+\pi^-\eta)$	0.107	1	0/0	0
$\omega\eta' \rightarrow (\pi^+\pi^-\pi^0)(\pi^+\pi^-\eta)$	0.284	5	0/0	0
$\rho\eta' \rightarrow (\pi^+\pi^-)(\pi^+\pi^-\eta)$	0.381	5	0/0	0
$2(\pi^+\pi^-)\eta$	22.6	5	0/0	0
$\eta K_s K^+\pi^- + c.c., K_s \rightarrow \pi^+\pi^-$	5.26	1	0/0	0

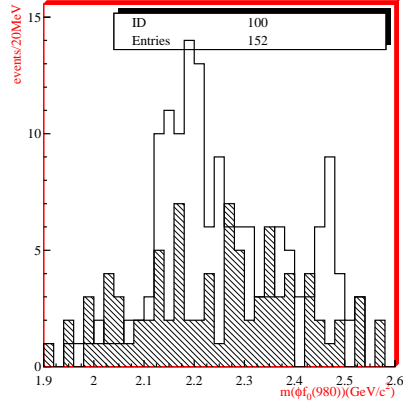


Figure 16: the $\phi f_0(980)$ invariant mass distribution from background events evaluated by η and $f_0(980)$ sidebands(hatched histogram).

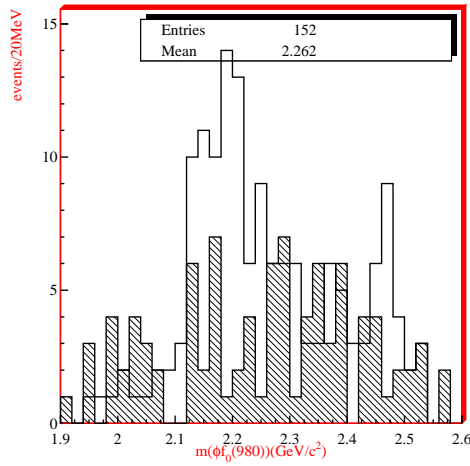


Figure 17: the $\phi f_0(980)$ invariant mass distribution from total background events evaluated by η , $f_0(980)$, and ϕ sidebands (hatched histogram)

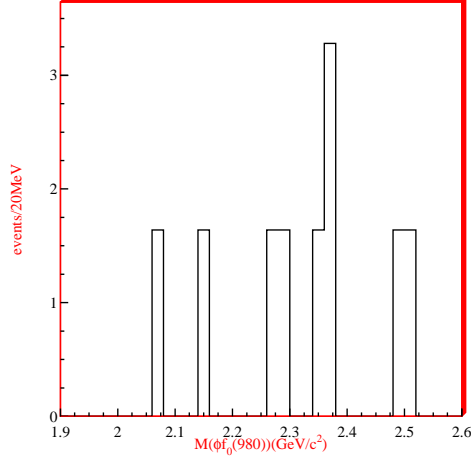


Figure 18: The $\phi f_0(980)$ invariant mass distribution from $J/\psi \rightarrow \text{anything}$

Table 3: Background channels without $\phi \rightarrow K^+K^-$ or $\eta \rightarrow \gamma\gamma$

Decay mode	Br (10^{-4})	MC (10^4)	Residual /efficiency(%)	Norm number
$\omega\eta' \rightarrow (\pi^+\pi^-\pi^0)(\pi^+\pi^-\gamma)$	0.48	2	0/0	0
$\gamma\eta\pi^+\pi^- \rightarrow \gamma(\pi^+\pi^-\pi^0)\pi^+\pi^-$	13.85	1	0/0	0
$\gamma K^* \bar{K}^* \rightarrow \gamma K_s \pi^0 K^+ \pi^-$,	6.15	5	0/0	0
$a_2(1320)\rho \rightarrow \eta\pi\rho \rightarrow 2(\pi^+\pi^-\pi^0)$	3.59	1	0/0	0
$2(\pi^+\pi^-\pi^0)$	162	10	0/0	0
$K^*(892)K(1430)^* + c.c.$ $\rightarrow K^+\pi^-K^-\pi^+\pi^0\pi^0$	1.33	1	0/0	0
$\omega f_1(1420) \rightarrow (\pi^+\pi^-\pi^0)(K^+K^-\pi^0)$	1.01	1	0/0	0
$\omega K^{*+}K^- \rightarrow (\pi^+\pi^-\pi^0)(K^+K^-\pi^0)$	7.87	1	0/0	0
$\phi f_1(1285) \rightarrow (\pi^+\pi^-\pi^0)(K^+K^-\pi^0)$	0004	10	0/0	0

histogram and the total sidebands histogram, and only the normalizations which are same for two histograms are floated. Thirdly a Breit-Wigner function folded with a gaussian function for the mass resolution of $0.012 \text{ GeV}/c^2$ is used as signal function.

The fitting results are shown in Fig. 20 and Fig. 21. The mass and width obtained are $m = 2.186 \pm 0.010(stat) \text{ GeV}/c^2$ and $\Gamma = 0.065 \pm 0.023(stat) \text{ GeV}/c^2$. The fit yields 52 ± 12 signal events and $-2\ln L = 78.6$. If we fit the invariant mass spectrum without the signal function (shown in Fig. 22 and Fig. 23), $-2\ln L = 116.0$. So the $\Delta\chi^2 = 18.7$ with a change of degree of freedom = 3, corresponding to a significance of 5.5σ .

Based on the signal events obtained by fitting the $\phi f_0(980)$ mass spectrum, the product branching ratio of $J/\psi \rightarrow \eta Y(2175)(Y(2175) \rightarrow \phi f_0(980), f_0(980) \rightarrow \pi\pi)$ can be determined according to the following relation:

$$Br(J/\psi \rightarrow \eta Y(2175)) \cdot Br(Y(2175) \rightarrow \phi f_0(980)) \cdot Br(f_0(980) \rightarrow \pi^+\pi^-) = \frac{N_{obs}}{\varepsilon \cdot Br(\eta \rightarrow \gamma\gamma) \cdot Br(\phi \rightarrow K^+K^-) \cdot N_{J/\psi}}$$

where N_{obs} is the signal events obtained from above fit, $N_{J/\psi}$ is the J/ψ total number, and ε is the detection efficiency of $J/\psi \rightarrow \eta Y(2175)(Y(2175) \rightarrow \phi f_0(980), f_0(980) \rightarrow \pi^+\pi^-)$ which is obtained from MC simulation (shown in Fig. 24). For $J/\psi \rightarrow \eta Y(2175)(Y(2175) \rightarrow \phi f_0(980), f_0(980) \rightarrow \pi\pi)$, supposing J^{PC} of $Y(2175)$ is 1^{--} , the Monte-Carlo generator which considers the angular distributions of $1^{--} \rightarrow 0^{-+} + 1^{--}, 1^{--} \rightarrow 1^{--} + 0^{++}$ is used to estimate the detection efficiency. In this analysis, N_{obs} is 48 ± 12 , $N_{J/\psi}$ is 5.77×10^7 , and ε is 1.52%. $Br(\eta \rightarrow \gamma\gamma)$ and $Br(\phi \rightarrow K^+K^-)$ are 39.38% and 49.2% respectively from PDG06. The branching ratio is then:

$$Br(J/\psi \rightarrow \eta Y(2175)) \cdot Br(Y(2175) \rightarrow \phi f_0(980)) Br(f_0(980) \rightarrow \pi^+\pi^-) = (3.06 \pm 0.71) \times 10^{-4}.$$

Here, the error is only statistical.

6.1.2 Using 3-order polynomial as background function

The fit is also performed by using a 3th-order polynomial as the background and a Breit-Wigner function folded with a gaussian function as the signal. The results are shown in Fig. 25. The mass and width obtained are $m = 2.182 \pm 0.010$ and $\Gamma = 0.073 \pm 0.024$. The fit yields 61 ± 14 signal events and $-2\ln L = 29.8$. If we fit the invariant mass spectrum without the signal function (shown in Fig.26), $-2\ln L = 61.0$. So the $\Delta\chi^2 = 15.6$ with a change of degree of freedom = 3, corresponding to a significance of 4.9σ .

According to the signal events obtained from above fits, the branching ratio is given as:

$$Br(J/\psi \rightarrow \eta Y(2175)) \cdot Br(Y(2175) \rightarrow \phi f_0(980)) Br(f_0(980) \rightarrow \pi^+\pi^-) = (3.59 \pm 0.82) \times 10^{-4}.$$

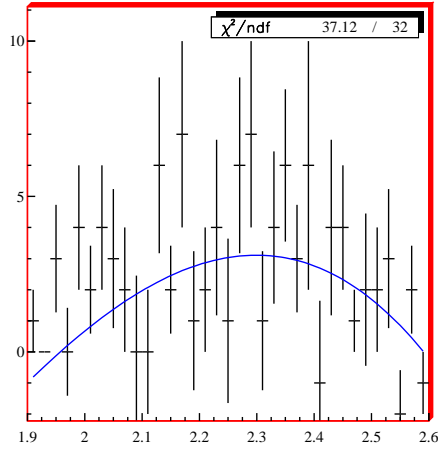


Figure 19: $\phi f_0(980)$ invariant mass distribution from the total sidebands events, the curve is a 3-order polynomial

MINUIT Likelihood Fit to Plots 103&0; 303&0
 Plot 103&0:
 File: mmy2175.hbk 9-SEP-2007 11:39
 Plot Area Total/Fit 151.00 / 151.00 Fit Status 3
 Func Area Total/Fit 144.92 / 144.92 E.D.M. 2.646E-08
 Likelihood = 78.6
 $\chi^2 = 78.2$ for 58 - 4 d.o.f., C.L. = 1.7%
 Individual Likelihoods: 22.7, 55.9
 Func convoluted with Gaussian of width 1.210E-02, intervals 50, sigma***
 Errors Parabolic Minos
 Function 1: phi0-nophase
 NORM 52.116 ± 11.77 - 0.000 + 0.000
 *NRM1/NORM 1.0000 ± 0.000 - 0.000 + 0.000
 MASS 2.1859 ± 9.978E-03 - 0.000 + 0.000
 WIDTH 6.52006E-02 ± 2.3167E-02 - 0.000 + 0.000
 *THRES 1.9200 ± 0.000 - 0.000 + 0.000
 Function 2: poly-bgshape-3d
 PARA1 2.9247 ± 0.2590 - 0.000 + 0.000
 *AR1/AREA 0.50000 ± 0.000 - 0.000 + 0.000

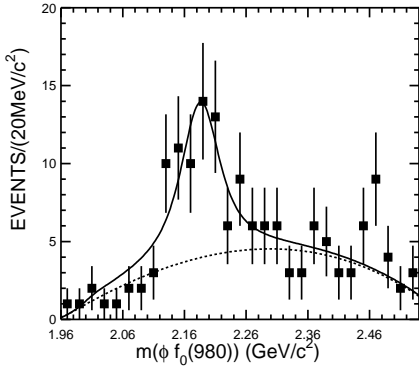


Figure 20: The $\phi f_0(980)$ invariant mass and the curve is fitting result with one resonance

MINUIT Likelihood Fit to Plots 103&0; 303&0
 Plot 303&0:
 File: side-v2.hbk 9-SEP-2007 11:39
 Plot Area Total/Fit 86.000 / 86.000 Fit Status 3
 Func Area Total/Fit 93.007 / 93.007 E.D.M. 2.646E-08
 Likelihood = 78.6
 $\chi^2 = 78.2$ for 58 - 4 d.o.f., C.L. = 1.7%
 Individual Likelihoods: 22.7, 55.9
 Func convoluted with Gaussian of width 1.210E-02, intervals 50, sigma***
 Errors Parabolic Minos
 Function 1: phi0-nophase
 NORM 52.116 ± 11.77 - 0.000 + 0.000
 *NRM1/NORM 1.0000 ± 0.000 - 0.000 + 0.000
 MASS 2.1859 ± 9.978E-03 - 0.000 + 0.000
 WIDTH 6.52006E-02 ± 2.3167E-02 - 0.000 + 0.000
 *THRES 1.9200 ± 0.000 - 0.000 + 0.000
 Function 2: poly-bgshape-3d
 PARA1 2.9247 ± 0.2590 - 0.000 + 0.000
 *AR1/AREA 0.50000 ± 0.000 - 0.000 + 0.000

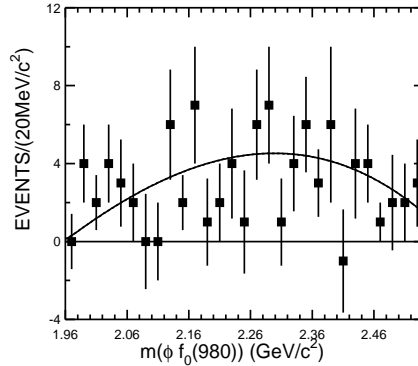


Figure 21: The $\phi f_0(980)$ invariant mass from sidebands and the curve is fitting results simultaneously

MINUIT Likelihood Fit to Plots 103&0; 303&0
 Plot 103&0;
 File: mny2175.hbk 9-SEP-2007 11:48
 Plot Area Total/Fit 151.00 / 151.00 Fit Status 3
 Func Area Total/Fit 118.93 / 118.93 E.D.M. 2.270E-05
 Likelihood = -116.0
 $\chi^2 = 115.6$ for 58 - 1 d.o.f., C.L.=0.723E-03%
 Individual Likelihoods: 51.1, 65.0
 Func convoluted with Gaussian of width 1.210E-02, intervals 50, sigma***
 Errors Parabolic Minos
 Function 1: poly-bgshape-3d
 *PARA1 3.7399 ± 0.2424 - 0.000 + 0.000
 *AR1/AREA 0.50000 ± 0.000 - 0.000 + 0.000

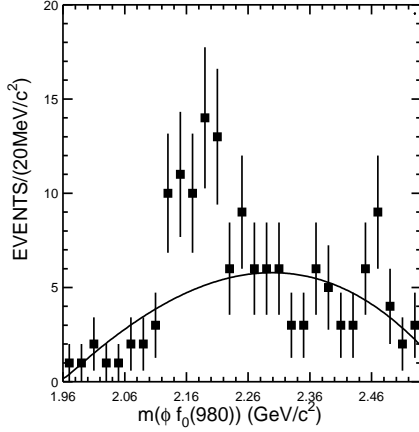


Figure 22: The $\phi f_0(980)$ invariant mass and the curve is fitting result without resonances

MINUIT Likelihood Fit to Plots 103&0; 303&0
 Plot 303&0;
 File: side-v2.hbk 9-SEP-2007 11:48
 Plot Area Total/Fit 86.000 / 86.000 Fit Status 3
 Func Area Total/Fit 118.93 / 118.93 E.D.M. 2.270E-05
 Likelihood = -116.0
 $\chi^2 = 115.6$ for 58 - 1 d.o.f., C.L.=0.723E-03%
 Individual Likelihoods: 51.1, 65.0
 Func convoluted with Gaussian of width 1.210E-02, intervals 50, sigma***
 Errors Parabolic Minos
 Function 1: poly-bgshape-3d
 *PARA1 3.7399 ± 0.2424 - 0.000 + 0.000
 *AR1/AREA 0.50000 ± 0.000 - 0.000 + 0.000

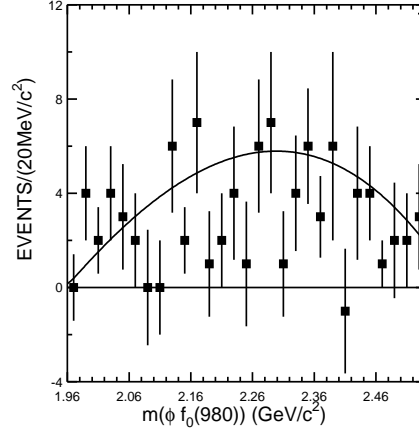


Figure 23: The $\phi f_0(980)$ invariant mass from sidebands and the curve is fitting results simultaneously

MINUIT Likelihood Fit to Plots
 File: mny2175-v2.hbk 27-AUG-2007 12:53
 Plot Area Total/Fit 2769.0 / 2769.0 Fit Status 0
 Func Area Total/Fit 2766.9 / 2767.6 E.D.M. 1.00
 Likelihood = -99.5
 $\chi^2 = 104.7$ for 31 - 5 d.o.f., C.L.=0.211E-08%
 Func convoluted with Gaussian of width 1.210E-02, intervals 50, sigma***
 Errors Parabolic Minos
 Function 1: phi0-nophase-ncoeff
 *NORM 2921.0 ± 52.20 - 0.000 + 0.000
 *MASS 2.1911 ± 9.8833E-04 - 0.000 + 0.000
 *WIDTH 7.38954E-02 ± 1.9929E-03 - 0.000 + 0.000
 *THRES 1.9200 ± 0.000 - 0.000 + 0.000
 Function 2: poly-3-ord
 *PARA1 1111.7 ± 4.1434E-02 - 0.000 + 0.000
 *PARA2 -562.00 ± 2.0910E-02 - 0.000 + 0.000

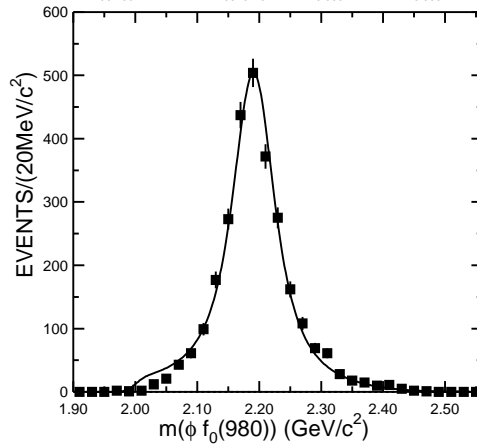


Figure 24: The $\phi f_0(980)$ spectrum from MC resonance sample (by angular distribution generator)

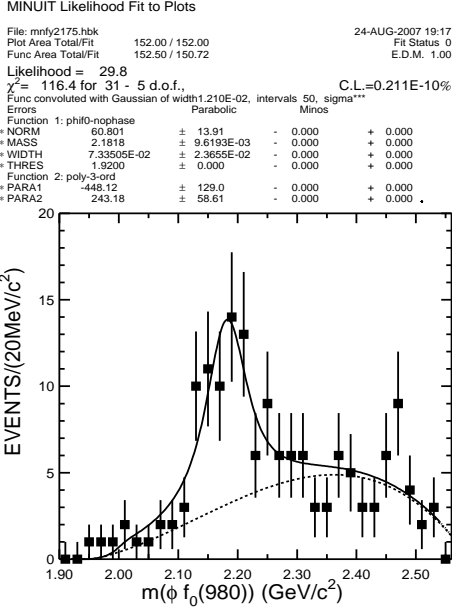


Figure 25: The $\phi f_0(980)$ invariant mass and the curve is fitting result with one resonance and 3-order polynomial

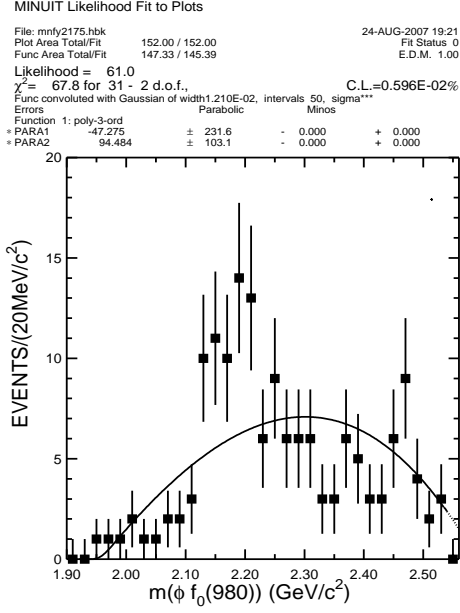


Figure 26: The $\phi f_0(980)$ invariant mass and the curve is fitting results with only 3-order polynomial

6.2 Fitting with two resonances

In the $\phi f_0(980)$ invariant mass spectrum, a small bump at around 2.47 GeV/c^2 can be seen. In BABAR's initial results, the $\phi f_0(980)$ cross section measured in the $K^+K^-\pi^+\pi^-$ final state shows structures around 2.15 GeV and possibly 2.4 GeV [9]. Therefore, we tried the fit of $\phi f_0(980)$ invariant mass spectrum with two non-interfering Breit-Wigner functions, in which, the mass and width of second peak are fixed to 0.077 GeV/c^2 and 2.47 GeV , the BABAR fit results[9].

6.2.1 Using sidebands contribution as background shape

We fit the $\phi f_0(980)$ invariant mass spectrum histogram and the total sidebands histogram simultaneously. The fit curves are shown in Fig. 27 and Fig. 28. The mass and width obtained are $m = 2.186 \pm 0.010(\text{stat}) \text{ GeV}/c^2$ and $\Gamma = 0.065 \pm 0.022(\text{stat}) \text{ GeV}/c^2$. The fit yields 47 ± 14 events for first peak and 22 ± 11 events for second peak. $-2\ln L = 72.2$. If we fit the invariant mass spectrum without the Breit-Wigner function for the first peak (shown in Fig.29 and Fig.30), $-2\ln L = 113.7$. So for the first peak the $\Delta\chi^2 = 20.75$ with a change of degree of freedom = 3, corresponding to a significance of 5.8 σ . For the second peak, comparing

Fig. 29 and Fig. 22, $\Delta\chi^2 = 1.05$ with a change of degree of freedom = 1, corresponding to a significance of 1.5σ .

According to the signal events obtained from above fit, the branching ratio is given as:

$$Br(J/\psi \rightarrow \eta Y(2175)) \cdot Br(Y(2175) \rightarrow \phi f_0(980)) Br(f_0(980) \rightarrow \pi^+\pi^-) = (2.77 \pm 0.82) \times 10^{-4}.$$

6.2.2 Using 3-order polynomial as background function

When treating the background as a 3-order polynomial function (constrain the start point and the end point to be zero), the fit curves are shown in Fig. 31. The mass and width obtained are $m = 2.186 \pm 0.010$ and $\Gamma = 0.085 \pm 0.027$. The fit yields 69 ± 23 signal events for first peak and 19 ± 16 signal events for second peak. $-2\ln L = 26.9$. If we fit the invariant mass spectrum without the first Breit-Wigner signal function (shown in Fig. 32), $-2\ln L = 60.9$. So for the first peak $\delta\chi^2 = 17$ with a change of degree of freedom = 3, corresponding to a significance of 5.2σ . For the second peak, comparing Fig. 32 and Fig. 26, $\Delta\chi^2 = 1.45$ with a change of degree of freedom = 1, corresponding to a significance of 1.7σ .

According to the signal events obtained from above fit, the branching ratio is given as:

$$Br(J/\psi \rightarrow \eta Y(2175)) \cdot Br(Y(2175) \rightarrow \phi f_0(980)) Br(f_0(980) \rightarrow \pi^+\pi^-) = (4.06 \pm 1.35) \times 10^{-4}.$$

From above four kinds of fit results, we conclude that first peak $Y(2175)$ has a significance of about 5σ , second peak is not significant. The mass, width and branching ratio obtained from four fits are consistent within the error. We choose the first fit results as central values and estimate their errors in following.

7 Systematic error

The systematic errors are considered as below:

- MDC tracking efficiency. This has been measured from clean channels like $J/\psi \rightarrow \Lambda\bar{\Lambda}$, $\psi(2S) \rightarrow \pi^+\pi^- J/\psi$, and $J/\psi \rightarrow \mu^+\mu^-$. It is found that the Monte Carlo simulation agrees with data within 1 – 2% for each charged track. Therefore, 8% for the channels with four charged tracks in the final states are taken as the systematic error from MDC tracking.

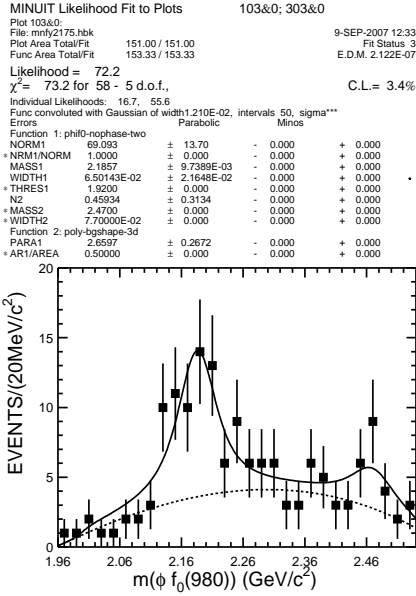


Figure 27: The $\phi f_0(980)$ invariant mass and the curve is fitting result with two resonances

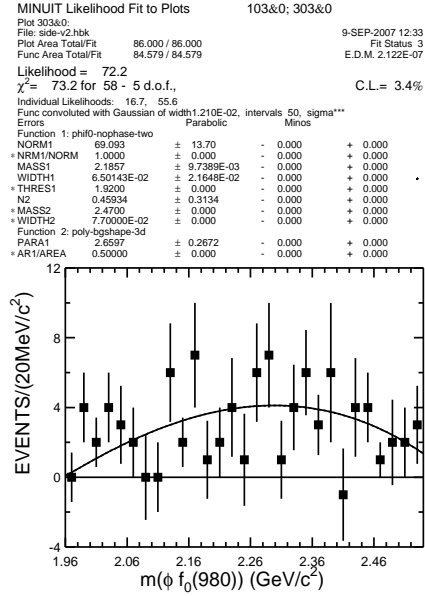


Figure 28: The $\phi f_0(980)$ invariant mass from sidebands and the curve is fitting results simultaneously

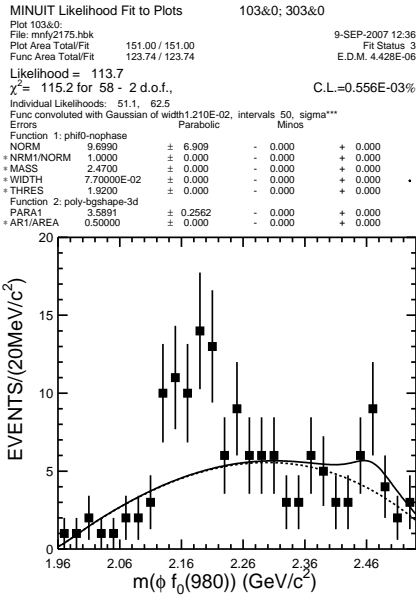


Figure 29: The $\phi f_0(980)$ invariant mass and the curve is fitting result with one resonance(mass and width fixed to BABAR's second peak results)

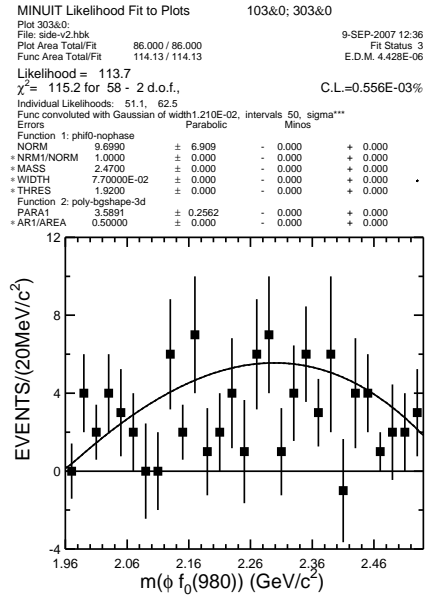


Figure 30: The $\phi f_0(980)$ invariant mass from sidebands and the curve is fitting results simultaneously

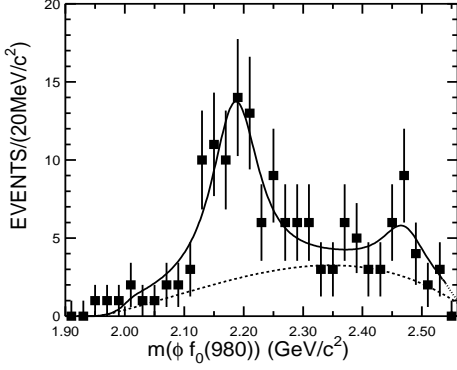
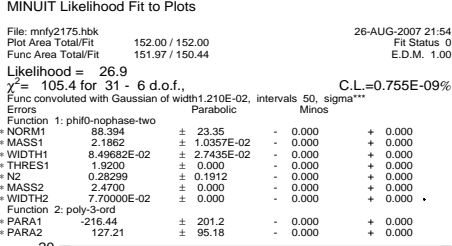


Figure 31: The $\phi f_0(980)$ invariant mass and the curve is fitting result with two resonances(one peak fixed) and 3-order polynomial

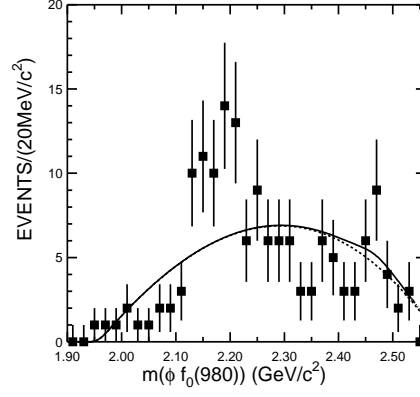
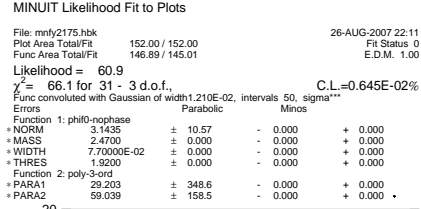


Figure 32: The $\phi f_0(980)$ invariant mass and the curve is fitting results with one resonance(fixed) and 3-order polynomial

- Photon detection efficiency. This has been studied using different methods with $J/\psi \rightarrow \rho^0 \pi^0$ events [10]. The difference between data and Monte Carlo simulation is about 2% for each photon in the photon energy region from 0.1 to 0.8 GeV/c^2 . 4% is taken to be the system error from photon efficiency.
- Particle identification (PID). It has been studied from $J/\psi \rightarrow K^+ K^- \pi^0$, the efficiency of PID from data is consistent with that from Monte Carlo simulation. The average difference is less than 2% for K particle, while for the π particle the error can be neglected. So 4% are taken as the systematic error in this analysis.
- The uncertainty of intermediate decays. The uncertainty of branching ratios for $\eta \rightarrow \gamma\gamma$ and $\phi \rightarrow K^+ K^-$ is taken as 0.66% and 1.22% from PDG06.
- Kinematic fit. The kinematic fit is used to reduce background. Using the same method for estimating the systematic error as in Ref. [11], the decay mode $J/\psi \rightarrow 3(\pi^+ \pi^-) \pi^0$ and $J/\psi \rightarrow 2(\pi^+ \pi^-) \pi^0$ and $J/\psi \rightarrow 3(\pi^+ \pi^-)$ are also analyzed in Ref. [12]. Their efficiency difference of the kinematic fit for data and MC are 5.5%, 4.3% and 8.7%. Since the

channel in this analysis are similar to the decay of $J/\psi \rightarrow 2(\pi^+\pi^-)\pi^0$, the systematic errors are taken as 4.3%.

- Invariant mass spectrum fitting. The uncertainty is caused by fitting range, background shape and different bin width. Table 4 list the biggest changes of branching ratio, mass and width after changing the fitting range from $1.96 - 2.54$ to $1.98 - 2.54$, $1.96 - 2.52$, background function from 3-order polynomial to 2-order polynomial, 4-order polynomial and bin width from 20MeV to 15MeV, 10MeV.
- The total number of J/ψ events. The number of J/ψ is $(57.7 \pm 2.72) \cdot 10^6$, determined from J/ψ inclusive 4-prong events [14]. The uncertainty is taken as a systematic error in branching ratio measurement.

Table 5 list the systematic errors from all above sources, and the total systematic errors is the sum of them added in quadrature.

8 summary

Based on a sample of 5.8×10^7 J/ψ events taken with BESII detector, $J/\psi \rightarrow \eta\phi f_0(980)$ has been analyzed via $\eta \rightarrow \gamma\gamma$, $\phi \rightarrow K^+K^-$ and $f_0(980) \rightarrow \pi^+\pi^-$. A structure is observed with about 5σ significance in the $\phi f_0(980)$ invariant mass spectrum. A fit with a Breit-Wigner function yields a mass $m = 2.186 \pm 0.010(stat) \pm 0.005(syst)$ GeV/ c^2 , a width $\Gamma = 0.065 \pm 0.023(stat) \pm 0.006(syst)$ GeV/ c^2 and a product branching ratio $Br(J/\psi \rightarrow \eta Y(2175)) \cdot Br(Y(2175) \rightarrow \phi f_0(980)) \cdot Br(f_0(980) \rightarrow \pi^+\pi^-) = (3.06 \pm 0.71(stat) \pm 0.45(syst)) \times 10^{-4}$.

References

- [1] B.Aubert et al., Phys. Rev. D **74**, 091103(R) (2006).
- [2] Gui-Jun Ding, Mu-lin Yan, hep-ph/0611319

Table 4: Systematic from invariant mass spectrum fitting.

	Fitting range	Bg shape	bin width
BR	1.92%	7.69%	3.85%
Mass	0.000	0.003	0.001
width	0.001	0.002	0.002

Table 5: Systematic from different sources.

Sources	Branching ratio(%)	Mass(GeV)	Width(Gev)
MDC Tracking	8		
Photon efficiency	4		
PID	4		
4C-fit	4.3		
Intermediate decays			
$\eta \rightarrow \gamma\gamma$	0.66		
$\phi \rightarrow K^+K^-$	1.22		
Invariant mass spectrum fitting	8.81	0.003	0.003
J/ψ total number	4.72		
Fitting bias		0.004	0.005
total	14.8	0.005	0.006

- [3] Gui-Jun Ding, Mu-lin Yan, hep-ph/0701047
- [4] Z.G. Wang, hep-ph/0610171
- [5] J.Z. Bai *et al.*, (BES Collab.), Nucl. Instr. and Meth. A458(2001) 627
- [6] C. Zhang, *et al.*, in: J. Rossback(Ed.). HEACC'92, XVth Int. Conf. on High Energy Accelerators, Hamburg, Germany, July 20–24, 1992, P.409
- [7] M. Ablikim *et al.*, (BES Collab), Nucl. Instr. and Meth. A 552 (2005) 344
- [8] J.Z. Bai *et al.*, Phys. Lett. B **476**,25-32 (2000).
- [9] B.Aubert *et al.*, hep-ex/0704.0630v1
- [10] S.M. Li *et al.*, High Energy Phys. Nucl. Phys.(in Chinese).
- [11] J.Z. Bai *et al.*, Phys. Rev. D **70**, 012005 (2004).
- [12] J.Z. Bai *et al.*, Phys. Lett. B610, 192-198(2005).
- [13] Particle Data Group,J.Phys. G: Nucl. Part. Phys. 33(2006) 1.
- [14] S.S. Fang *et al.*, High Energy Phys. Nucl. Phys. **27**, 277 (2003) (in Chinese).